



High-performance heralded squeezing gate with quantum network modulesXing Lei,¹ Jieli Yan ¹, Jianrong Deng,¹ Zhihui Yan ^{1,2,*} and Xiaojun Jia¹¹*State Key Laboratory of Quantum Optics and Quantum Optics Devices, Institute of Opto-Electronics, Shanxi University, Taiyuan 030006, People's Republic of China*²*Collaborative Innovation Center of Extreme Optics, Shanxi University, Taiyuan 030006, People's Republic of China*

(Received 22 August 2024; revised 1 October 2024; accepted 18 November 2024; published 9 December 2024)

The quantum gate and quantum memory are building blocks for distributed quantum computation. It is a longstanding goal to implement high-fidelity quantum operations with quantum network modules to process and store quantum information. Here we propose a high-performance heralded squeezing gate with quantum network modules. By distributing one submode of the entangled state to a quantum network module, a heralded squeezing gate is realized, and the fidelity is enhanced by the heralding filter. Furthermore, the heralded squeezing gate can be realized between two network modules, where quantum operation can be manipulated by another quantum network module. Our scheme is scalable for quantum network modules and provides a direct reference for potential practical applications of distributed quantum computation.

DOI: [10.1103/PhysRevA.110.062604](https://doi.org/10.1103/PhysRevA.110.062604)**I. INTRODUCTION**

Quantum computation can solve some special problems that classical computation cannot, and larger-scale quantum computation is key for practical applications [1], which are hindered by decoherence [2–4]. In addition to fault-tolerant quantum error correction [5–8], distributed quantum computation with quantum network modular architecture is one possible solution to overcome the decoherence problem of large-scale quantum computation, where the quantum gates between spatially separated modules are the essential resource of distributed quantum computation [9–11]. Thus, the quantum gates with quantum modules are the building blocks of distributed quantum computation.

Quantum teleportation is the reliable transfer of a quantum state with entanglement and has also been demonstrated to transfer a quantum state between light and matter modules [12]. Quantum networks are composed of quantum nodes and quantum channels, where quantum nodes are used to store and process quantum information, and quantum channels are used to transfer quantum information [13–15]. Meanwhile, quantum teleportation can establish the quantum connectivity in network modules with interactions between photons and atoms [16]. Therefore, it is required to connect multiple different spatially separated quantum modules by quantum teleportation to implement quantum operations between quantum network modules. However, it remains challenging to implement and manipulate quantum gates with quantum modules [17–20].

Here we propose a high-performance heralded squeezing gate with quantum network modules. The quantum operations between different modules can be implemented by connecting these quantum modules with distributed quantum

entanglement and manipulating the quantum operation with quantum teleportation. The squeezing gate is one of the essential quantum gates for continuous-variable quantum information. In this scheme, a heralded squeezing gate is realized between two spatially separated quantum network modules, where the output state of the squeezing gate can be manipulated by another module based on quantum teleportation. Furthermore, a high-performance squeezing gate is demonstrated and the gate fidelity is improved without requiring more squeezed ancillary vacuum [21]. A heralded filter is developed to improve the fidelity during the distribution scale. In contrast to previous work, in our scheme the necessary atomic memory node is introduced in the quantum gate, and the heralding filter is used to improve the fidelity within the distribution distance and memory time. With the development of quantum networks, the quantum memory network stage is distinguished by incorporating the memory capability of the end nodes [13]. The atomic ensemble is employed in the squeezing gate to process and memorize the quantum state. However, the fidelity of the squeezing gate with quantum memory is limited because of the imperfect quantum memory. Thus, the heralding filter is used to improve the fidelity of the heralded squeezing gate with quantum memory, and high-fidelity squeezing gate can be realized between any quantum network modules within a distance of 1 km.

The paper is organized as follows. The scheme of a heralded squeezing gate with quantum nodes is proposed in Sec. II. The results of a heralded squeezing gate between light-atom or atom-atom network modules are analyzed in Sec. III. A brief summary is provided in Sec. IV.

II. SCHEME OF A HERALDED SQUEEZING GATE WITH QUANTUM NODES

The heralded squeezing operation can be implemented by distributing the entanglement to two quantum modules. The

*Contact author: zhyang@sxu.edu.cn

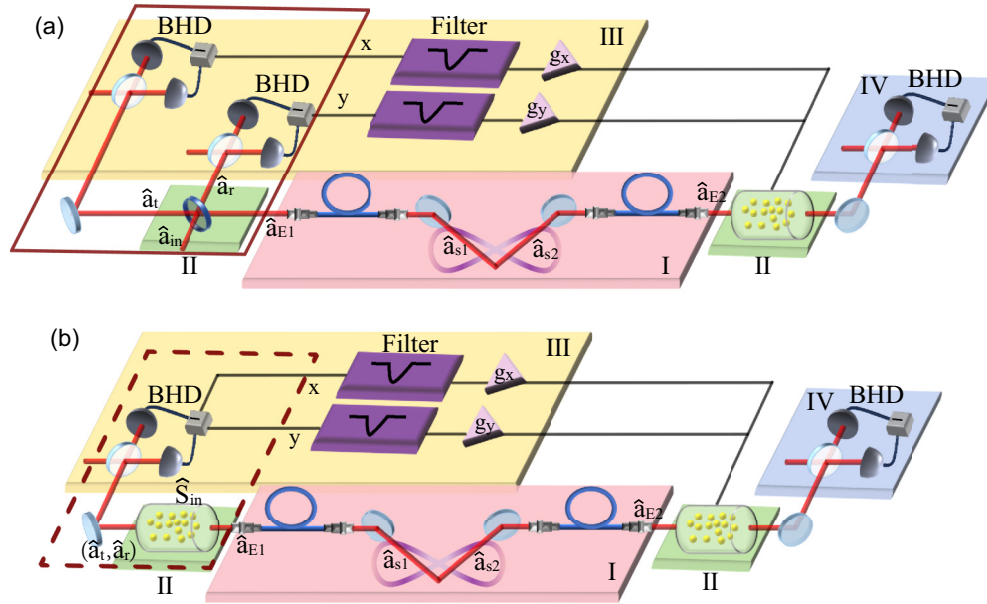


FIG. 1. The scheme of the heralded squeezing gate through heralded noiseless linear amplification. (a) The squeezing gate is realized by light-atom network modules. (b) The squeezing gate is realized by atom-atom network modules. Part I is the generation and distribution of quantum state. Part II is the quantum nodes. Part III is the feedforward system, which consists of the measurement system and the heralding filter, while the atomic node and measurement system in the dashed line can be replaced by the light system and measurement system on the left part in the solid line. Part IV is the verification system.

quantum memory is also needed in each module and can remotely manipulate the function of the herald squeezing gate [9], where the quadrature components of the output squeezed state and target squeezing can be manipulated by changing the quantum memory efficiency. The atom network module is based on a cavity-enhanced quantum memory node, where not only is the memory efficiency increased but also the noise is suppressed. Thus, the heralded squeezing gate can be realized with one memory node in a single module and two memory nodes distributed across two modules. The scheme of the heralded squeezing gate is shown in Fig. 1. Part I is the generation and distribution of the quantum state. Part II represents the quantum nodes. Part III is the feedforward system, which consists of the measurement system and the heralding filter, while the atomic node and measurement system in the dashed line can be replaced by the light system and the measurement system on the left part of the solid line. Part IV is the verification system. The quantum resources of the heralded squeezing gate include a pair of entangled optical modes and one [Fig. 1(a)] or two [Fig. 1(b)] atomic nodes.

In part I, the distributed quantum nodes are interconnected by a pair of entangled beams through long-distance fibers. In teleportation-based quantum computation, the beam splitter plays a key role in quantum teleportation, where the input and entangled states are coupled for measurement and feed-forward of quantum teleportation. For the light-atom network modules, the interference between the entangled state and the input state occurring on the beam splitter (BS) is used for measurement and feedback in Fig. 1(a). The atom-based quantum memory in Fig. 1(b) is treated as a beam splitter interaction, similar to the optical beam splitter in Fig. 1(a). The transmission and reflection parts in the quantum memory process correspond to the transmitted and release optical modes,

which can be distinguished at different times. In addition, their quadratures consist of feedback components. The other entangled beam on the right is memorized in the atomic node, where its memory efficiency needs to be kept at a maximum for optimal performance. The squeezing gate on the atomic node is contingent upon the feedback of the amplitude and phase quadratures through a heralding filter. The logical gate can be memorized in the atomic node during memory time T_0 , where it decays with the atomic spin-wave decoherence rate. The information in the atomic node is transferred to the light for verification in part IV. The quadratures and variance of the logical gate are obtained via measurement on a balanced homodyne detector (BHD), and the performance of the squeezing gate can be evaluated in terms of fidelity. Finally, the enhancement of module distance and memory time with a heralding filter is analyzed in the squeezing gate.

A. Generation and distribution of the entangled state

Quantum entangled optical fields are fundamental resources for quantum teleportation [22,23], as well as for applications in quantum logical gates [24,25], quantum dense coding [26,27], and quantum secret sharing [28]. Optical parametric amplifiers are widely used to generate squeezed and entangled states for quantum information science [29]. The fidelity of the squeezing gate composed of an entangled state is significantly superior to that composed of the squeezed state in the regime of low noise and higher detection efficiency, and the entangled state is more sensitive to low noise and detection efficiency. Therefore, the entangled state is more conducive to practical applications, enabling the realization of a higher-fidelity squeezing gate. For example, for cesium (Cs), the wavelength of 852 nm corresponds to

both the atomic transition lines and one of the fiber windows. The initial optical entangled modes (\hat{a}_{s1} and \hat{a}_{s2}) are generated by an amplitude-quadrature squeezed beam and a phase-quadrature squeezed beam at a BS of 50:50, with the relative phase at 0, and are distributed to remote modules via fibers in opposite directions. Thus, the module distance is twice the fiber length. The distributed entangled modes (\hat{a}_{E1} and \hat{a}_{E2}) are used in two remote modules. The optical modes (\hat{a}_{si}) through a fiber can be mathematically expressed as $\hat{a}_{Ei} = \sqrt{\eta_2}\hat{a}_{si} + \sqrt{(1-\eta_2)}\hat{a}_{vi} + \hat{n}_{gi}$, $i \in 1, 2$, where \hat{S}_{in} and \hat{a}_{in} are the input states of heralded squeezing gates with (with-out) quantum memory. \hat{a}_{vi} and \hat{n}_{gi} represent the vacuum noise and guided-acoustic-wave Brillouin scattering noise operators through fibers in opposite directions. $V(\hat{n}_{gi}) = \eta_2\xi l I$ is the variance of guided-acoustic-wave Brillouin scattering noise, ξ is the transmission loss coefficient, l is the fiber length, and I is the power of light. The reflection part and the transmission part of the beam splitter (\hat{a}_r and \hat{a}_t) are measured by balanced homodyne detectors and feedforward, which are illustrated in the figure. The total transmission efficiency (η_2) is determined by the fiber coupled efficiency (η_3) and the fiber transmission efficiency, and the fiber transmission efficiency is given by $\eta_2 = \eta_3 10^{-\xi l/10}$, where $\eta_3 = 85\%$ and $\xi = 2.5$ dB/km under realistic conditions. The realization of the squeezing gate is predicated on the correlation between the entangled beams. The specific relationship of these entangled beams is crucial for the implementation of the squeezing gate, which can be expressed as

$$\begin{aligned}\hat{x}_{E2} - \hat{x}_{E1} &= \sqrt{2\eta_2}e^{-r}\hat{x}_0 + \sqrt{1-\eta_2}\hat{x}_v + \hat{x}_g, \\ \hat{y}_{E2} + \hat{y}_{E1} &= \sqrt{2\eta_2}e^{-r}\hat{y}_0 + \sqrt{1-\eta_2}\hat{y}_v + \hat{y}_g,\end{aligned}\quad (1)$$

where $\hat{x}_v = \hat{x}_{v2} - \hat{x}_{v1}$, $\hat{x}_g = \hat{x}_{g2} - \hat{x}_{g1}$, $\hat{y}_v = \hat{y}_{v2} + \hat{y}_{v1}$, $\hat{y}_g = \hat{y}_{g2} + \hat{y}_{g1}$, and \hat{x}_i and \hat{y}_i , $i \in 0, v1, v2, g1, g2$, are the amplitude and phase quadratures of the optical state, which correspond to the coherent state, vacuum state, and guided-acoustic-wave Brillouin scattering noise. Thus, the entangled optical modes can be distributed to two quantum network modules for the heralded squeezing gate.

B. Cavity-enhanced quantum nodes

The quantum memory is pivotal for implementing the heralded squeezing gate on the atomic node [13]. Cavity-enhanced quantum memory, in which an atomic cell is placed in a ring bow cavity to achieve high fidelity, serves as an exemplary atomic node [30]. The mechanism of electromagnetically induced transparency in Cs is particularly well-suited for quantum memory applications. A Λ -type energy-level structure is employed, where a weak signal and a strong control beam are associated with the energy-level transitions of the light and atom coupling. The interaction Hamiltonian between atoms and light in the cavity-enhanced model can be formulated as the BS type ($\hat{H} = \kappa\hat{a}^\dagger\hat{S} + \kappa\hat{a}\hat{S}^\dagger$), where \hat{a} represents the light mode, and where \hat{S} is the collective atomic spin wave, as described by the Stokes operator. The effective light-atom coupling coefficient is given by ($\kappa = \sqrt{N}\mu\Omega/\Delta$), which is a function of the number of atoms (N), the Rabi frequency (Ω), and the light-atom coupling constant (μ). The amplitude and phase quadratures of the atoms are associated with

the y and z components of the Stokes operator, respectively, and can be described as $\hat{X}_A = (\hat{S} + \hat{S}^\dagger)/\sqrt{2} = \hat{S}_y/\sqrt{(\hat{S}_x)}$ and $\hat{Y}_A = (\hat{S} - \hat{S}^\dagger)/\sqrt{2}i = \hat{S}_z/\sqrt{(\hat{S}_x)}$. The dynamic evolution of the light state and collective atomic spin wave can be shown by the quantum Langevin dynamics equations [31]

$$\begin{aligned}\frac{d\hat{a}(t)}{dt} &= -\gamma\hat{a}(t) - i\kappa(t)\hat{S}(t) + \sqrt{2\gamma_1}\hat{A}^{\text{in}}(t) + \sqrt{2\gamma_2}\hat{A}_v^{\text{in}}(t), \\ \frac{d\hat{S}(t)}{dt} &= -\gamma_0\hat{S}(t) - i\kappa(t)\hat{a}(t) + \sqrt{2\gamma_0}\hat{S}_v(t),\end{aligned}\quad (2)$$

where γ_0 is the spin-wave decoherence rate, $\gamma = \gamma_1 + \gamma_2$, γ_1 is the coupling rate to the cavity of the input and output fields, and γ_2 is the decay rate of the intracavity loss. The initial mode is tailored to an optimal pulse shape for quantum memory, which can maximize the transfer of information onto the atoms within the cavity. The optimal shape is determined by the atom and light coupling rates and the decay rates of both the atoms and the cavity. In addition to the noise originating from intracavity losses (L), the extra noise in the system also includes four-wave mixing (FWM) noise, which depends on the intensity of the control beam. In the cavity-enhanced model, the FWM noise can be effectively suppressed by antiresonance with the cavity, while simultaneously enhancing the light-atom interaction by ensuring that the signal mode is resonant with the cavity. The signal and control modes are set in two orthogonal polarization directions and coupled into the cavity via the polarization beam splitter. The resonance of both the signal and control beams with the cavity can be synchronized by manipulating the temperature of a birefringent crystal, which results in different optical path lengths for orthogonal polarizations. The signal and FWM beams have the same polarization in the cavity and can maintain the resonance condition in the cavity. The FWM beam is near the antiresonant without the crystal, whereas the control beam is near the resonance. Therefore, the FWM noise suppression factor can be increased by birefringent crystals. During the writing process, the signal optical mode from light is mapped on the atomic node. Then, the information can be memorized during the lifetime of the atomic node with the signal and control beams off. Finally, the light mode is retrieved from the atomic node, and its pulse shape function can be calculated from the Langevin dynamics equation. The total efficiency is a product of the writing and reading efficiencies. The writing and reading efficiencies are the ratio of the integrated area of the pulse shape between the conversion of the light and the atomic node, which are expressed as

$$\begin{aligned}\eta_w(0) &= \frac{\gamma_1\kappa^2}{(\kappa^2 + \gamma_0\gamma_1 + \gamma_0\gamma_2)(\gamma_0 + \gamma_1 + \gamma_2)}, \\ \eta_r(T_0) &= \frac{(\gamma_1\kappa^2e^{-\gamma_0T_0} - \gamma_1\gamma_0^2e^{-(\gamma_1+\gamma_2)T_0})^2}{\gamma_1\kappa^2e^{-\gamma_0T_0}(\kappa^2 + \gamma_0\gamma_1 + \gamma_0\gamma_2)(\gamma_0 + \gamma_1 + \gamma_2)},\end{aligned}\quad (3)$$

The atomic spin wave and read efficiency decay with the exponential function of memory time. The final information can be verified by measuring the reading part with imperfect reading efficiency on the BHD. The cavity-enhanced quantum memory enables the heralded squeezing gate between the atomic nodes.

C. Active feedforward

The active feedforward enables the heralded squeezing gate, with distributed entangled modes and cavity-enhanced quantum memory. In the system of light-atom network modules, the feedback modes consist of the transmission part ($\hat{a}_t = \sqrt{\eta_w}\hat{a}_{E1} + \sqrt{1-\eta_w}\hat{a}_{in}$) and the reflection part ($\hat{a}_r = \sqrt{1-\eta_w}\hat{a}_{E1} + \sqrt{\eta_w}\hat{a}_{in}$) through the BS. Furthermore, when employing atom-atom network modules, the transmission part from the reading out from the atomic node (\hat{a}_t), the reflection part (\hat{a}_r), and the spin wave of the other atomic node (\hat{S}_r) can be written as

$$\begin{aligned}\hat{a}_t &= \sqrt{\eta_t}(\sqrt{\eta_w}\hat{S}_A - \sqrt{1-\eta_w} - L\hat{a}_{E1} + \sqrt{L}\hat{a}_{v1}) \\ &\quad + \sqrt{1-\eta_t}\hat{a}_{t1}, \\ \hat{a}_r &= \sqrt{\eta_r}(\sqrt{\eta_r}(\sqrt{\eta_w}\hat{a}_{E1} - \sqrt{1-\eta_w} - L\hat{S}_A \\ &\quad + \sqrt{L}\hat{S}_{v1} + \hat{S}_{z1}) + \sqrt{1-\eta_r}\hat{a}_v) + \sqrt{1-\eta_r}\hat{a}_{r1}, \\ \hat{S}_r &= \sqrt{\eta_{w2}}\hat{a}_{E2} + \sqrt{1-\eta_{w2}} - L\hat{S}_{in} + \sqrt{L}\hat{S}_v + \hat{S}_z.\end{aligned}$$

The amplitude and phase quadratures of the transmission part must be measured as the feedback components and feedforward to the atomic node. The quadratures of the reflection mode (\hat{X}_2, \hat{Y}_2) can be rewritten by the feedback quadratures (\hat{x}_t, \hat{y}_r) of the optical modes \hat{a}_t and \hat{a}_r as $\hat{X}_2 = c_1 * \hat{x}_t + x + \hat{X}_{n2}$ and $\hat{Y}_2 = c_2 * \hat{y}_r + y + \hat{Y}_{n2}$, where $c_1 = \langle \hat{x}_t, \hat{X}_2 \rangle / V(\hat{x}_t)$, $c_2 = \langle \hat{y}_r, \hat{Y}_2 \rangle / V(\hat{y}_r)$, $x = \langle \hat{X}_2 \rangle - c_1 \langle \hat{x}_t \rangle$, $y = \langle \hat{Y}_2 \rangle - c_2 \langle \hat{y}_r \rangle$, $\hat{X}_{n2} = V(\hat{X}_2) - c_1^2 * V(\hat{x}_t)$, and $\hat{Y}_{n2} = V(\hat{Y}_2) - c_2^2 * V(\hat{y}_r)$.

Next, the heralding filter is used to improve its fidelity. The method is based on a virtual cutoff of the postselection filter acting on the measurement records. The probabilistic filter is used on the measurement records with the filter strength g_f , resulting in the probability distribution of the output state. The probability distribution of the input coherent state can be given as $f(\alpha_m) = \exp[(|\alpha_m|^2 - \alpha_c^2)(1 - \frac{1}{g_f})]$ if $|\alpha_m| < \alpha_c$ and as $f(\alpha_m) = 1$ if $|\alpha_m| \geq \alpha_c$, where α_c is the cutoff. The Q function of the quantum state with the amplitude of the input state (α_0) can be written as $Q'(\alpha_m) = \frac{1}{\sqrt{2\pi}} \exp(-|\alpha_m - \alpha_0|^2)$, and the function will change to $Q(\alpha_m) = f(\alpha_m)Q'(\alpha_m)$ through the heralding filter, where α_m is the amplitude of the measurement state. The success probability can be given by

$$\begin{aligned}P &= \iint_{|\alpha_m| < \frac{\alpha_c}{g_f}} \frac{g_f^2}{\sqrt{2\pi}} e^{-\frac{1}{2}(\alpha_m - g_f\alpha_0)^2} e^{\frac{1}{2}(g_f^2 - 1)(\alpha_0^2 - \frac{\alpha_c^2}{g_f^2})} d^2\alpha_m \\ &\quad + \iint_{|\alpha_m| \geq \frac{\alpha_c}{g_f}} \frac{g_f^2}{\sqrt{2\pi}} e^{-\frac{1}{2}(g_f\alpha_m - \alpha_0)^2} d^2\alpha_m.\end{aligned}\quad (4)$$

Moreover, the average value and variance of the amplitude and phase quadratures need to be integrated through the probability distribution after the heralding filter. The average value and variance change as $\langle \hat{x}_t^f \rangle = g_f \langle \hat{x}_t \rangle$ and $V(\hat{y}_r^f) = g_f V(\hat{y}_r)$. The amplitude and phase quadratures of the final state can be expressed as

$$\begin{aligned}\hat{X}_o &= \hat{X}_2 + g_x \hat{x}_t = (c_1 + g_x) * \hat{x}_t^f + x + \hat{X}_{n1}, \\ \hat{Y}_o &= \hat{Y}_2 + g_y \hat{y}_r = (c_2 + g_y) * \hat{y}_r^f + y + \hat{Y}_{n2}.\end{aligned}\quad (5)$$

The feedback gains can be calculated by $g_x = (\langle \hat{X}_o \rangle - x) / (g_f * \langle \hat{x}_t \rangle) - c_1$ and $g_y = (\langle \hat{Y}_o \rangle - y) / (g_f * \langle \hat{y}_r \rangle) - c_2$. The variances of the amplitude and phase quadratures are $V(\hat{X}) = \langle \hat{X}^2 \rangle - \langle \hat{X} \rangle^2$ and $V(\hat{Y}) = \langle \hat{Y}^2 \rangle - \langle \hat{Y} \rangle^2$. The squeezing gate is achieved under the unity gain conditions $V(\hat{X}_o) = e^{2*r}$ and $V(\hat{Y}_o) = e^{-2*r}$, where r is the target squeezing parameter. The writing efficiency, which determines the initial state (\hat{S}_{in}) and the entangled mode, also influences the target squeezing level with $\eta_w = 1 / (1 + e^{-2*r})$ [32]. The fidelity is used to evaluate the squeezing gate, and it describes the overlap of the ideal state and the realistic state. The fidelity of a single-mode Gaussian state can be expressed in terms of the ideal and output covariance values (V_i and V_o):

$$F = \frac{2}{(\sqrt{\Delta + \Lambda} - \sqrt{\Lambda})} \exp[-(\delta\langle\alpha\rangle)^T (V_i + V_o)^{-1} \delta\langle\alpha\rangle], \quad (6)$$

where $\Delta = \det(V_i + V_o)$, $\Lambda = (\det V_i - 1)(\det V_o - 1)$, and $\delta\langle\alpha\rangle$ is the relative average displacement.

III. RESULTS OF HERALDED SQUEEZING GATE BETWEEN NETWORK MODULES

Quantum interconnects link and distribute coherent quantum information between systems and across different length scales. Interconnects enable the construction of powerful quantum computers to execute quantum algorithms by connecting elements within a quantum subsystem, between quantum processors, and between quantum and classical computers [10]. The heralded squeezing gate enables the input coherent state to be squeezed on the atomic network module, and is the building block of complex quantum computation. The fidelity of a quantum system is a critical criterion for evaluating the system. It is essentially a metric that quantifies how closely a quantum operation resembles its ideal version. In practical terms, the fidelity reflects the performance of a quantum gate and is crucial for assessing its reliability. First, the system of the entangled light and an atomic node or two entangled atomic nodes are prepared to achieve the squeezing gate through feedback. Then, a postselection filter and an optimal cavity are used to optimize the fidelity and suppress extra noise, respectively. Finally, the fidelity of the squeezing gate with memory time and transmission distance is analyzed under a cavity-enhanced quantum memory model. In the system, we assume that two squeezed states have identical squeezing levels and that all the BSs of the equipment are lossless. The cavity is a ring bow structure with the birefringent crystal placed at one waist and the atomic cell placed at the other waist. The writing efficiency of the feedforward part is related to the target squeezing level and can be manipulated by the power of the control light. The writing efficiency, reading efficiency, and transmission efficiency maintain the maximum values at 95%, 90%, and 92%, respectively, for the gate measurement without atomic decay of the memory time. Under optimal noise suppression conditions within the cavity, the FWM noise of two atomic nodes is 0.02%. The total transmission of measurement is 90%, which is caused by the measurement system.

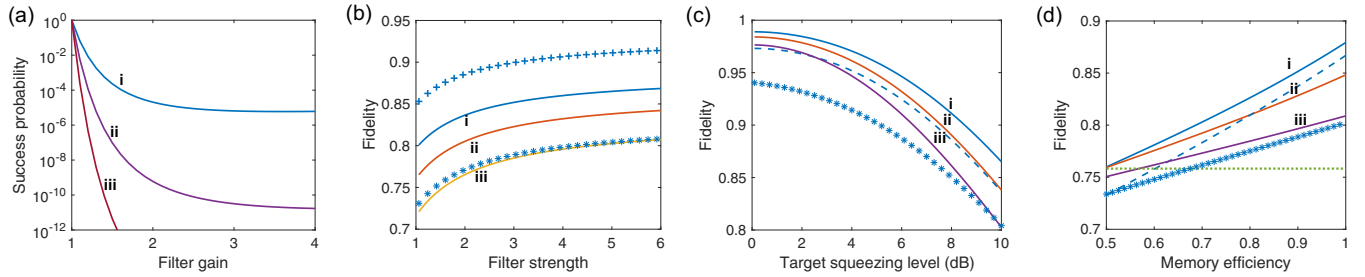


FIG. 2. Dependence of squeezing gate fidelity with system limit. The solid line represents the system with one atomic node, and the star line represents the system with two atomic nodes beyond the same condition of line i. (a) The relationship between success probability and filter strength, the lines i, ii and iii with respect to the different cutoffs of 3, 4, and 5. (b) The relationship between the fidelity of the squeezing gate and the filter strength. The three lines i, ii, and iii correspond to the input squeezing levels with 10, 8, and 6 dB. (c) The relationship between the fidelity of the squeezing gate and the target squeezing level. The filter strength of 3 is shown by the dashed line. (d) The relationship between fidelity and memory efficiency of the memorized atomic node. The green dotted line represents the benchmark.

The fidelity can be enhanced with a larger filter strength; however, this comes at the cost of a larger cutoff [33]. It is important to balance the filter strength with the system cutoff to achieve the desired fidelity. In the following, we analyze the performance of the atomic nodes in the system. The dependence of the squeezing gate fidelity on the system factor is shown in Fig. 2. The success probability decreases with increasing filter strength as shown in Fig. 2(a), and the different cutoffs of 3, 4, and 5 are also analyzed. The fidelity of the squeezing gate with filter strength is analyzed with different input squeezing levels in Fig. 2(b). Three solid lines, i, ii, and iii, in the next three figures of Fig. 2 correspond to the squeezing levels of 10, 8, and 6 dB, respectively, and show the fidelity with one atomic node. They all show that the fidelity is efficiently improved by increasing the filter strength. The star line is the fidelity with filter strength by using two atomic nodes, and its fidelity is limited by memory efficiency and measurement loss. The relationship between fidelity and the target squeezing level is analyzed in Fig. 2(c). The dashed line is under the condition of a 10-dB input squeezing level and $g_f = 3$. The star line is under the condition of two atomic nodes. Thus, the fidelity decreases with increasing target squeezing level, and the fidelity with one atomic node is greater than that with two atomic nodes. It is also verified that the fidelity is enhanced by greater filter strength. The fidelity is always higher than the benchmark, which is the boundary of the coherent state. Otherwise, the fidelity can be enhanced by increasing the memory efficiency of the atomic node, which is used for memorizing the squeezing gate, and their relationship under three input squeezing levels of 10, 8, and 6 dB is shown in Fig. 2(d). Considering the condition close to the benchmark, the target squeezing level is 10 dB. The lines higher than the benchmark indicate that the squeezing gate is achieved. Overall, the fidelity is efficiently improved by increasing the filter strength, despite the reduction in success probability. The fidelity is lower to achieve a higher target squeezing level, and the fidelity can also be enhanced by the greater memory efficiency of the atomic node. The fidelity can reach 98% with a target squeezing level of 3 dB and $g_f = 5$. Therefore, the fidelity of the heralded squeezing gate is effectively enhanced by proper filter strength and target squeezing level, and memory efficiency can further improve the fidelity.

The fidelities of the heralded squeezing gate with the module distance and memory time are analyzed with respect to the filter strength in the system. Next, the target squeezing level is 10 dB for a more obvious phenomenon. The relationship between the fidelity and the module distance with one atomic node (two atomic nodes) is shown in Fig. 3(a) [Fig. 3(b)] with a memory time of 100 ns. Lines i, ii, and iii correspond to three different input squeezing levels of 10, 8, and 6 dB. The dashed line is under the condition of $g_f = 3$. The dashed line represents the benchmark. The lines together show that the fidelity decreases with the module distance with different input squeezing levels. The fidelity is enhanced with a better input squeezing level, and the communication distance is efficiently prolonged by the heralding filter. The memory time is another important performance metric for evaluating the system. The information will exponentially decay during the memory time [$\eta(t) = \eta_w(0) * \exp(-t/T_0)$]. Here we consider that the lifetime of the Cs atomic node (T_0) reaches 1 s [34]. The logical gate can be memorized in the atomic node for the lifetime corresponding to the decoherence of the atomic node. The fidelity of the squeezing gate with one atomic node (two atomic nodes) is shown in Fig. 3(c) [Fig. 3(d)] with a module distance of 50 m. Lines i, ii, and iii are under the condition of three different input squeezing levels of 10, 8, and 6 dB, and the dashed line represents the benchmark. The dashed line shows the fidelity with $g_f = 3$ compared with the solid line i. The heralded filter can effectively enhance the fidelity, which can surpass the classical benchmark within the range of 1060 m (420 m) distribution distance in Fig. 3(a) [Fig. 3(b)]. The fidelity can reach 0.865 (0.795) with the filter strength of 5 and the fidelity of 0.852 (0.782) is obtained with the filter strength of 3 under the condition that memory time is 500 ns between light-atom network modules (atom-atom network modules) in Fig. 3(c) [Fig. 3(d)]. Therefore, the scheme can effectively improve the fidelity of the quantum squeezing gate within the distribution distance and memory time. In addition, the bandwidth of the squeezed vacuum state up to 11 dB is 36 MHz for the optical quantum state [21]. For atomic memory, there has been great progress in broadband quantum memory, and the bandwidth of electromagnetically induced transparency can reach 660 MHz [35], which satisfies the bandwidth requirement of squeezed optical fields.

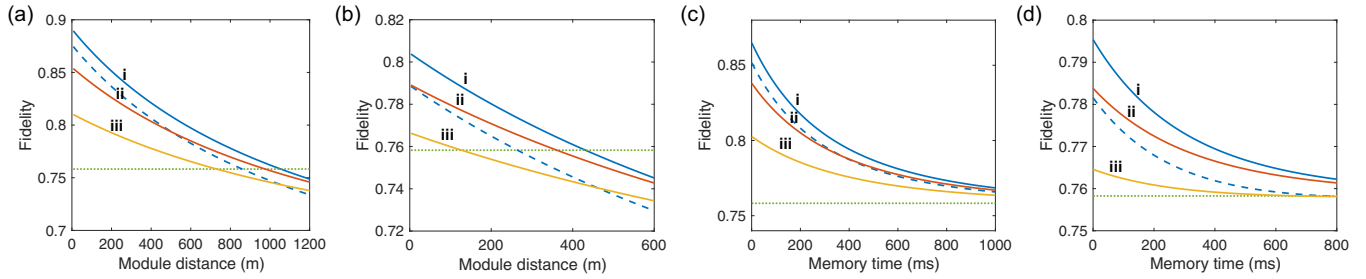


FIG. 3. Dependence of squeezing gate fidelity with module distance and memory time. (a), (b) The fidelity with the module distance. (c), (d) The fidelity with the memory time. (a), (c) The squeezing gate with one atomic node. (b), (d) The squeezing gate with two atomic nodes. The lines i, ii, and iii correspond to three different input squeezing levels with 10, 8, and 6 dB. The dashed line shows the fidelity with a filter strength of 3 compared to the solid line i. The green dotted line represents the benchmark.

Furthermore, the bandwidth of Raman in atomic systems can reach 1.8 GHz [36] for matching broadband squeezed states.

IV. CONCLUSION

In this paper, we propose a scheme of a high-performance heralded squeezing gate between network modules with a heralding filter. In this way, the squeezing gate can be distributed and memorized between the light and atom network modules. The heralded squeezing gate fidelity can obviously be enhanced within the module distance and atomic memory time, and the heralded squeezing gate can be realized between two network modules. In one-way quantum computation, arbitrary Gaussian quantum computation can be implemented sufficiently by single-mode and two-mode gates [37,38]. The heralded filter can be used in the two-mode quantum gates between two modules to construct a universal quantum gate set, which is essential for distribution quantum computation. This scheme is scalable with module number, and it allows the interconnection of more quantum network

modules with multipartite entanglement [28]. Moreover, the Gaussian state is well understood for quantum information and is the essential building block for continuous-variable quantum information processing [39]. This technique can be applied to non-Gaussian states and provides a promising pathway for high-fidelity gate operations and continuous-variable distributed quantum computations [21]. The heralded quantum teleporter, which is capable of processing an arbitrary input state, makes it possible to construct a universal quantum teleporter [40]. Therefore, this scheme can be applied for not only non-Gaussian states but also arbitrary input states.

ACKNOWLEDGMENTS

This research was supported by the National Outstanding Youth Foundation of China (62122044); China National Funds for Distinguished Young Scientists (61925503); National Natural Science Foundation of China (62135008); the National Key Research and Development Program of China (No. 2022YFA1404500); and the Fund for Shanxi “1331 Project” Key Subjects Construction.

-
- [1] M. V. Larsen, X. Guo, C. R. Breum, J. S. Neergaard-Nielsen, and U. L. Andersen, *Nat. Phys.* **17**, 1018 (2021).
- [2] T. D. Ladd, F. Jelezko, R. Laflamme, Y. Nakamura, C. Monroe, and J. L. O’Brien, *Nature (London)* **464**, 45 (2010).
- [3] F. Arute, K. Arya, R. Babbush, D. Bacon, J. C. Bardin, R. Barends, R. Biswas, S. Boixo, F. G. S. L. Brandao, D. A. Buell *et al.*, *Nature (London)* **574**, 505 (2019).
- [4] H. S. Zhong, H. Wang, Y. H. Deng, M. C. Chen, L. C. Peng, Y. H. Luo, J. Qin, D. Wu, X. Ding, Y. Hu *et al.*, *Science* **370**, 1460 (2020).
- [5] R. Acharya, I. Aleiner, R. Allen, T. I. Andersen, M. Ansmann, F. Arute, K. Arya, A. Asfaw, J. Atalaya, R. Babbush *et al.*, *Nature (London)* **614**, 676 (2023).
- [6] V. V. Sivak, A. Eickbusch, B. Royer, S. Singh, I. Tsioutsios, S. Ganjam, A. Miano, B. L. Brock, A. Z. Ding, L. Frunzio *et al.*, *Nature (London)* **616**, 50 (2023).
- [7] Z. Ni, S. Li, X. Deng, Y. Cai, L. Zhang, W. Wang, Z. B. Yang, H. Yu, F. Yan, S. Liu *et al.*, *Nature (London)* **616**, 56 (2023).
- [8] R. S. Gupta, N. Sundaresan, T. Alexander, C. J. Wood, S. T. Merkel, M. B. Healy, M. Hillenbrand, T. Jochym-O’Connor, J. R. Wootton, T. J. Yoder *et al.*, *Nature (London)* **625**, 259 (2024).
- [9] D. Awschalom, K. K. Berggren, H. Bernien, S. Bhave, L. D. Carr, P. Davids, S. E. Economou, D. Englund, A. Faraon, M. Fejer *et al.*, *PRX Quantum* **2**, 017002 (2021).
- [10] D. D. Awschalom, H. Bernien, R. Brown, A. Clerk, E. Chitambar, A. Dibos, J. Dionne, M. Eriksson, B. Fefferman, G. D. Fuchs *et al.*, Technical Report ANL-22/83 (2022), doi:10.2172/1900586.
- [11] Z. Chen, L. Sun, and C. L. Zou, *Sci. Bull.* **68**, 961 (2023).
- [12] Y. A. Chen, S. Chen, Z. S. Yuan, B. Zhao, C. S. Chuu, J. Schmiedmayer, and J. W. Pan, *Nat. Phys.* **4**, 103 (2008).
- [13] S. Wehner, D. Elkouss, and R. Hanson, *Science* **362**, eaam9288 (2018).
- [14] Y. Lei, F. K. Asadi, T. Zhong, A. Kuzmich, C. Simon, and M. Hosseini, *Optica* **10**, 1511 (2023).
- [15] A. I. Lvovsky, B. C. Sanders, and W. Tittel, *Nat. Photon.* **3**, 706 (2009).
- [16] H. J. Kimble, *Nature (London)* **453**, 1023 (2008).
- [17] N. Huo, Y. Liu, J. Li, L. Cui, X. Chen, R. Palivela, T. Xie, X. Li, and Z. Y. Ou, *Phys. Rev. Lett.* **124**, 213603 (2020).

- [18] S. Li, X. Pan, Y. Ren, H. Liu, S. Yu, and J. Jing, *Phys. Rev. Lett.* **124**, 083605 (2020).
- [19] Z. Yan, L. Wu, X. Jia, Y. Liu, R. Deng, S. Li, H. Wang, C. Xie, and K. Peng, *Nat. Commun.* **8**, 718 (2017).
- [20] K. S. Choi, A. Goban, S. B. Papp, S. J. van Enk, and H. J. Kimble, *Nature (London)* **468**, 412 (2010).
- [21] J. Zhao, K. Liu, H. Jeng, M. Gu, J. Thompson, P. K. Lam, and S. M. Assad, *Nat. Photon.* **14**, 306 (2020).
- [22] H. Yonezawa, T. Aoki, and A. Furusawa, *Nature (London)* **431**, 430 (2004).
- [23] M. Huo, J. Qin, J. Cheng, Z. Yan, Z. Qin, X. Su, X. Jia, C. Xie, and K. Peng, *Sci. Adv.* **4**, eaas9401 (2018).
- [24] S. Liu, Y. Lou, Y. Chen, and J. Jing, *Phys. Rev. Lett.* **128**, 060503 (2022).
- [25] X. Wang, J. Fu, S. Liu, Y. Wei, and J. Jing, *Optica* **9**, 663 (2022).
- [26] Y. Chen, S. Liu, Y. Lou, and J. Jing, *Phys. Rev. Lett.* **127**, 093601 (2021).
- [27] S. Liang, J. Cheng, J. Qin, J. Li, Y. Shi, Z. Yan, X. Jia, C. Xie, and K. Peng, *Phys. Rev. Lett.* **132**, 140802 (2024).
- [28] Y. Qin, J. Cheng, J. Ma, D. Zhao, Z. Yan, X. Jia, C. Xie, and K. Peng, *Phys. Rev. Res.* **6**, 033036 (2024).
- [29] X. Zuo, Z. Yan, Y. Feng, J. Ma, X. Jia, C. Xie, and K. Peng, *Phys. Rev. Lett.* **124**, 173602 (2020).
- [30] L. Ma, X. Lei, J. Yan, R. Li, T. Chai, Z. Yan, X. Jia, C. Xie, and K. Peng, *Nat. Commun.* **13**, 2368 (2022).
- [31] Q. Y. He, M. D. Reid, E. Giacobino, J. Cviklinski, and P. D. Drummond, *Phys. Rev. A* **79**, 022310 (2009).
- [32] K. Liu, J. Li, R. Yang, and S. Zhai, *Opt. Express* **28**, 23628 (2020).
- [33] J. Zhao, J. Y. Haw, T. Symul, P. K. Lam, and S. M. Assad, *Phys. Rev. A* **96**, 012319 (2017).
- [34] O. Katz and O. Firstenberg, *Nat. Commun.* **9**, 2074 (2018).
- [35] J. Wolters, G. Buser, A. Horsley, L. Béguin, A. Jöckel, J.-P. Jahn, R. J. Warburton, and P. Treutlein, *Phys. Rev. Lett.* **119**, 060502 (2017).
- [36] P. S. Michelberger, T. F. M. Champion, M. R. Sprague, K. T. Kaczmarek, M. Barbieri, X. M. Jin, D. G. England, W. S. Kolthammer, D. J. Saunders, J. Nunn *et al.*, *New J. Phys.* **17**, 043006 (2015).
- [37] R. Ukai, S. Yokoyama, J.-i. Yoshikawa, P. van Loock, and A. Furusawa, *Phys. Rev. Lett.* **107**, 250501 (2011).
- [38] X. Su, S. Hao, X. Deng, L. Ma, M. Wang, X. Jia, C. Xie, and K. Peng, *Nat. Commun.* **4**, 2828 (2013).
- [39] C. Weedbrook, S. Pirandola, R. García-Patrón, N. J. Cerf, T. C. Ralph, J. H. Shapiro, and S. Lloyd, *Rev. Mod. Phys.* **84**, 621 (2012).
- [40] J. Zhao, H. Jeng, L. O. Conlon, S. Tserkis, B. Shajilal, K. Liu, T. C. Ralph, S. M. Assad, and P. K. Lam, *Nat. Commun.* **14**, 4745 (2023).